Microscopic ergodicity breaking governs the emergence and evolution of elasticity in glass-forming nanoclay suspensions

Yihao Chen,[1] Simon A. Rogers,[2] Suresh Narayanan,[3]
James L. Harden,[4] and Robert L. Leheny[1]

[1]*Department of Physics and Astronomy, Johns Hopkins University, Baltimore, Maryland 21218, USA*

[2]*Department of Chemical and Biomolecular Engineering, University of Illinois Urbana-Champaign, Champaign, IL 61801, USA*

[3]*X-Ray Science Division, Argonne National Laboratory, Argonne, Illinois 60439, USA*

[4]*Department of Physics & CAMaR, University of Ottawa, Ottawa, Ontario K1N 6N5, Canada*

(Dated: October 9, 2020)

Abstract

We report a study combining x-ray photon correlation spectroscopy (XPCS) with *in situ* rheology to investigate the microscopic dynamics and mechanical properties of aqueous suspensions of the synthetic hectorite clay Laponite, which is composed of charged, nanometer-scale, disk-shaped particles. The suspensions, with particle concentrations ranging from 3.25 to 3.75 wt%, evolve over time from a fluid to a soft glass that displays aging behavior. The XPCS measurements characterize the localization of the particles during the formation and aging of the soft-glass state. The fraction of localized particles f_0 increases rapidly during the early formation stage and grows more slowly during subsequent aging, while the characteristic localization length r_{loc} steadily decreases. Despite the strongly varying rates of aging at different concentrations, both f_0 and r_{loc} scale with the elastic shear modulus G' in a manner independent of concentration. During the later aging stage, the scaling between r_{loc} and G' agrees quantitatively with a prediction of naive mode coupling theory. Breakdown of agreement with the theory during the early formation stage indicates the prevalence of dynamic heterogeneity, suggesting the soft solid forms through precursors of dynamically localized clusters.

I. INTRODUCTION

Colloidal suspensions, and many other soft-matter systems, go through an ergodic to non-ergodic transition that depends on the colloidal concentration, temperature, and other conditions [1–4]. Despite the various manifestations, all these non-erogodic states are thermodynamically out-of-equilibrium, which from the perspective of statistical mechanics implies their microscopic degrees of freedom are able to explore only part of the available phase space. Understanding of this transition, though far from complete, is important for the applications of soft matter in technologies, such as those related to the food and cosmetic industries. A complicating feature of the non-ergodic state is the dependence of material properties on the manner in which the state is entered and the subsequent sample history. Over the past few years, experimental and theoretical work on colloidal suspensions has shed light on the mechanisms underlying several examples of ergodic to non-ergodic transitions [1–4]. For instance, a suspension of monodisperse Brownian hard spheres has a glass transition at a volume fraction $\phi_g \approx 0.58$. Below ϕ_g hard-sphere suspensions behave as ergodic fluids, while above ϕ_g the suspensions are non-erogodic solids whose properties evolve slowly, a process known as aging [1, 5–7]. Dispersions of colloids with soft repulsive interactions similarly display a colloidal glass transition at a concentration that depends on the specifics of the interactions [8]. For colloidal systems with attractive interactions, a non-ergodic state can be achieved at much lower volume fractions through gel formation [2, 9, 10]. In all cases, the transition of colloidal systems into a non-ergodic state is typically accompanied by localization of the colloids [11] as well as the emergence of macroscopic elasticity [12, 13]. However, the way in which these two phenomena at very different length scales relate to each other is still unclear.

Particularly intriguing examples of colloidal systems that display an ergodic to non-ergodic transition are aqueous dispersions of the synthetic hectorite clay Laponite, which is composed of nanometer-sized, disk-shaped colloids. In aqueous suspension the faces of the Laponite platelets acquire a negative charge while the rims become positively charged. The resulting orientation-dependent interparticle interactions combined with the anisotropic particle shape endow Laponite dispersions with a rich state diagram as a function of particle concentration, pH, and ionic strength [14–19] that includes multiple arrested states with characteristic aging behavior [20–24]. In the absence of added salt, suspensions of

freshly dispersed Laponite particles at sufficient volume fraction and high pH gradually and spontaneously transition from fluid to soft glass with complex, age-dependent rheological properties [19, 25]. This process and the nature of the non-ergodic states of Laponite suspensions more broadly have been a topic of extensive study [17, 26].

In this paper, we report experiments employing x-ray photon correlation spectroscopy with *in-situ* rheometry (rheo-XPCS) on a set of Laponite suspensions of varying concentration during formation and aging of the soft-glass state. XPCS and rheometry track the evolution in the suspensions' particle-scale dynamics and mechanical properties, respectively. We take advantage of the unique capability with rheo-XPCS to obtain these results simultaneously on the same sample to make unambiguous, quantitative connections between the formation of the non-ergodic state, characterized microscopically by the localization of the particles, and the accompanying onset and growth of macroscopic elasticity. Since the material properties and aging behavior of Laponite suspensions can be strongly influenced by detailed aspects of the preparation protocol and storage conditions, this strategy of simultaneous XPCS and rheology on a single sample has particular value. Further, by exploiting recent advances in x-ray detector technology, we extend the dynamic range of the XPCS measurements over earlier studies to characterize the fast dynamics at the initial stage in the soft-glass formation.

The XPCS correlation function shows a two-step relaxation process as observed previously in dynamic light scattering (DLS) [27–29] and XPCS [30–32] experiments. The wave-vector dependence of the intermediate plateau in the correlation function shows that, with increasing time since dispersion of the Laponite in solution, an increasing fraction of the particles become dynamically arrested with increasingly restricted caged motion. The fraction of localized particles goes through two stages of growth with different rates. Comparison with the evolving macroscopic rheology indicates that the first stage coincides with initial formation of the soft-glass state and the second with its subsequent aging. During the formation stage, a small but rapidly growing fraction of the particles displays a finite localization length even while the elastic shear modulus of the suspensions remains close to zero, indicating strong heterogeneity with clusters of dynamically arrested particles. During the second stage, when the majority of particles are arrested, the growth rate of the localized fraction slows while the elastic modulus steadily increases. During this stage, the localization length of the particles and the elastic modulus obey a modified version of a

quantitative scaling relationship predicted by naive mode coupling theory [33, 34] that has previously been shown to connect the microscopic dynamics and rheology of concentrated thermoreversible nanocolloidal silica gels [35] and casein micelle gels [36]. This scenario is robust for all colloidal concentrations investigated, despite the strong variation in the pace of formation and aging with concentration. The apparent presence of a fraction of localized particles prior to any measurable elasticity calls for new theoretical investigation into the origin of the ergodic to non-ergodic transition of colloidal suspensions.

II. EXPERIMENTAL PROCEDURES

A. Sample preparation

Laponite clay (RD grade, BYK Additives GmbH) is composed of disk-shaped particles with 30 nm average diameter and 1 nm thickness. The clay was dried under vacuum at 80 °C for 12 hours before use. Appropriate quantities of the clay were added to deionized water, and the suspensions were placed in a sealed container and stirred until clear, which typically required 15 minutes. The suspensions were then filtered (0.45 μm pore size) to remove aggregates, leading to homogeneous suspensions with high pH (pH $\approx$ 10). The age of the samples t_w was taken as the time since filtration. Included in the study were suspensions with three weight fractions, C_w = 3.25 wt%, 3.5 wt%, and 3.75 wt%, which correspond to volume fractions $\phi = 0.125$, 0.135, and 0.144, respectively, assuming a density of the Laponite of 2.6 g/cm^3. All three concentrations fall in the range in which, in the absence of added salt, Laponite forms a soft-glass state [17].

B. Rheo-XPCS

Rheo-XPCS measurements were carried out at sector 8-ID of the Advanced Photon Source. The suspensions were loaded into a Couette cell of a stress-controlled rheometer (Anton Paar MCR 301) mounted on the beam line immediately after filtering. The Couette cell was composed of thin-walled polycarbonate and had a 5.5 mm inner radius and a 6.1 mm outer radius, enabling rheological tests in parallel with transmission small-angle x-ray scattering measurements, as described previously [37]. Exposure to air and drying of the sample were minimized by a solvent trap that enclosed the Couette cell. Measurements were

performed with the axis of the Couette cell oriented vertically and the horizontal incident beam directed radially through the center of the cell. A partially coherent x-ray beam of energy 10.9 keV (wavelength $\lambda = 1.14$ Å) and size 100×20 μm^2 (V $\times$ H) was focused vertically to a 3×20 μm^2 spot on the sample. Two area detectors 4.91 m after the sample were deployed to record the scattering at different frame rates. One detector (X-spectrum LAMBDA 750K) [38, 39], with a 1556×516 array of 55×55 μm^2 pixels, measured the scattering intensity at a frame rate of 20 fps over the range 0.02 nm$^{-1} < q < 0.65$ nm^{-1}, where $q = 4\pi \sin(\theta/2)/\lambda$ is the scattering wave vector at scattering angle θ. The other, a newly developed high-frame-rate detector (Rigaku UHSS-500K) [40], with a 1024×512 array of 76×76 μm^2 pixels, measured the scattering intensity over wave vectors 0.02 nm $^{-1} < q <$ 0.6 nm^{-1} at 5×10^4 fps to capture dynamics at shorter times.

To monitor the formation of the soft-solid state and its aging behavior both macroscopically and microscopically, we performed alternating rheometry and XPCS measurements in which each rheology test was followed by 5 measurements with the Rigaku detector for 100000 frames and one measurement with the LAMBDA detector for 10000 frames. To avoid effects of radiation damage to the sample, the rheometer was translated a small distance between each XPCS measurement, so that a new portion of the sample was irradiated in each measurement. The rheology tests were composed of a brief measurement of the complex shear modulus at frequency 0.1 Hz and strain amplitude 0.1%. Between each rheology test, the rheometer was held at zero shear rate for the XPCS measurements.

The microscopic dynamics captured by the XPCS measurements is characterized by the wave-vector-dependent intensity auto-correlation function

$$g_2(q,\tau) = \frac{\langle I(\mathbf{q},t)I(\mathbf{q},t+\tau)\rangle_t}{\langle I(\mathbf{q},t)\rangle_t^2}, \tag{1}$$

where $I(\mathbf{q},t)$ is the intensity at wave vector $\mathbf{q}$ and time t, τ is the delay time, and the brackets represent averages over time of a single measurement and over detector pixels in the vicinity of wave-vector magnitude q. The auto-correlation function is related to the dynamic structure factor $f(q,\tau)$ through the Siegert relation [41],

$$g_2(q,\tau) = 1 + bf^2(q,\tau) \tag{2}$$

where b is the Siegert factor, which varies weakly with wave vector and depends on instrumental factors such as the coherence of the incident beam, the solid angle subtended by a

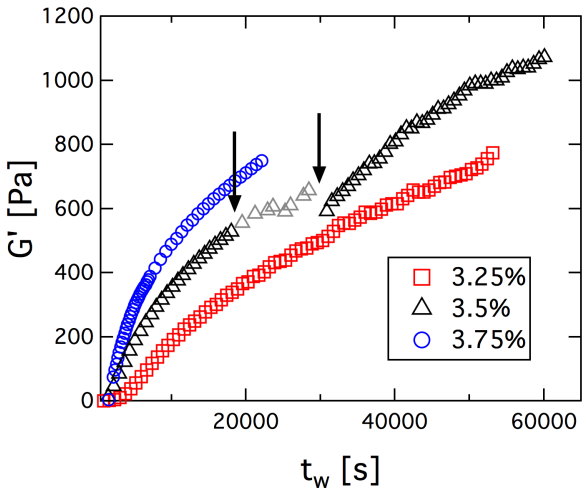

FIG. 1. Storage modulus G' as a function of age of Laponite suspensions with concentrations C_w = 3.25 wt% (red squares), 3.5 wt% (black triangles), and 3.75 wt% (blue circles). Measurements were performed at strain amplitude 0.1% and frequency 0.1 Hz. The suspension with C_w = 3.5 wt% was also subjected intermittently to larger-amplitude strains between ages of 18940 s and 29860 s to test for rejuvenation, as described in the text. The data in this range is shown in grey and bracketed by the arrows.

detector pixel, and the sample thickness [41]. In the rheo-XPCS measurements, the Siegert factor is affected by the addition at the detector of scattering from the front half and back half of the Couette cell when the incident beam is directed radially through the cell. To determine the Siegert factor for measurements with each detector in this scattering geometry, we performed measurements on two thin, static samples (Aerogel) separated by 11 mm to mimic the spacing between the front half and back half of the cell. The measurements confirmed that the scattering from the front and back of the cell added at the detector largely incoherently. The Siegert factor for the LAMBDA detector decreased from 0.088 to 0.079 with increasing q from 0.06 to 0.16 nm^{-1} and that for the Rigaku detector decreased from 0.061 to 0.055 over the same range.

III. RESULTS AND DISCUSSION

The Laponite suspensions at all three concentrations displayed characteristic aging behavior that proceeded at a rate that depends on the concentration. As shown in Fig. 1, the

storage modulus G' of each suspension grew gradually as a function of age t_w from essentially zero to about 1000 Pa during the duration of each experiment. (The rate of change of G' was sufficiently small in all cases that the mutation number [42] remained below 0.1 at all ages, indicating the linearity of the measurements.) Although the difference in colloidal concentration was less than 15% among the three samples, the growth of the storage modulus varied dramatically, especially when the age to achieve a certain storage modulus is considered. In the experiments on the suspensions with $C_w = 3.25$ wt% and 3.75 wt%, the samples were left undisturbed throughout the experiment except for the small-amplitude oscillatory shear applied at regular intervals to determine G'. In the experiment on the suspension with $C_w = 3.5$ wt%, the sample was subjected to an additional set of larger-amplitude shear deformations to characterize their effect on the aging. These deformations included a series of oscillatory shears with amplitudes ranging from 2% to 32% (five such tests at 0.5 Hz each for 40 s) beginning at $t_w = 18492$ s and culminated with 300 seconds of steady shear at shear rate 0.5 s^{-1} ending at $t_w = 29863$ s. As the results in Fig. 1 show, these deformations, particularly the steady shear, interrupted the growth in G', effectively "rejuvenating" the suspension. However, following these tests, the suspension resumed aging, and importantly, the nature of the growth in G' remained essentially unaltered.

Figure 2 displays the normalized XPCS correlation functions at wave vector $q = 0.077$ nm^{-1} measured on the suspension with $C_w = 3.25$ wt%. (For reference, the scattering intensity $I(q)$ of the sample at various ages is provided in Appendix A.) The correlation functions are obtained from combining the results from measurements with the high-frame-rate Rigaku detector, shown with solid symbols, and those with the LAMBDA detector, shown with open symbols. The data from the Rigaku detector is the mean of $f^2(q,\tau)$ from five measurements taken successively at a given age, and the data at $\tau < 10^{-2}$ s is further subject to a boxcar average to improve statistics. As the figure illustrates, the results from the two detectors match very well after normalization by the different Siegert factors. The shape of the correlation function indicates a two-step relaxation. Specifically, at the shortest τ, the correlation function appears to capture the final part of a fast, partial decay to a plateau that begins roughly at $\tau \approx 10^{-3}$ s and that extends over a range of delay times that increases with increasing age before the correlation function undergoes a second, terminal decay at larger τ. Such a two-step relaxation has been observed previously in DLS measurements on Laponite suspensions [20, 27, 32] and is a generic property of many glassy

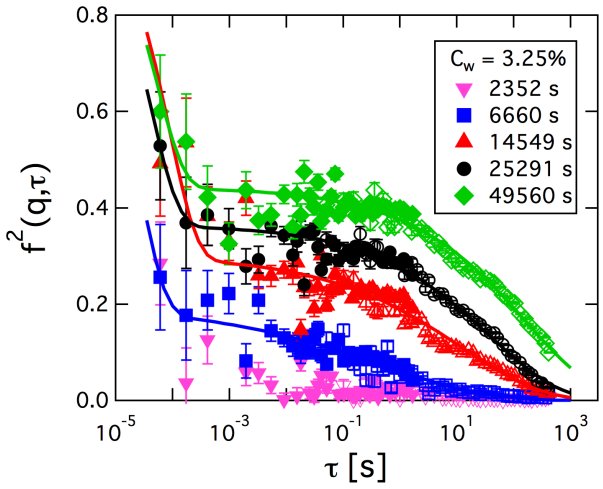

FIG. 2. Normalized XPCS correlation functions measured using the Rigaku (solid symbols) and LAMBDA (open symbols) detectors at wave vector q = 0.077 nm^{-1} at different ages of the suspension with C_w = 3.25 wt%. The solid lines depict the results of fits using Eq. (3).

systems [11, 35, 43]. The fast relaxation is interpreted as corresponding to diffusive motion of the particles within the cages formed by their neighbors, and the increase in the plateau value with increasing age implies increasingly restricted localization of the particles. The terminal relaxation at larger delay time is associated with slow, cage-breaking processes or with strain in response to heterogeneous internal stress in the disordered soft solid (see Appendix B for details).

This two-step relaxation is accurately described by a functional form for $f(q,\tau)$ comprised of a fast exponential decay followed by a slow stretched-exponential decay,

$$f(q,\tau) = (1-A)\exp[-\tau/\tau_1] + A\exp\left[-(\tau/\tau_2)^{\beta}\right] \tag{3}$$

where τ_1 and τ_2 are the relaxation times of the fast and slow decays, respectively, β is the stretching exponent, and A, which is known as the non-ergodicty parameter, sets the value of the intermediate plateau between the fast and slow relaxations. The solid lines in Fig. 2 display the results of fits using Eq. (3). The properties of the terminal relaxation, specifically the wave-vector and age-dependent trends of τ_2 and β, are consistent with previous studies, which have addressed the behavior of this relaxation and its interpretation in detail [27, 28]. We describe our results for τ_2 and β along with further details about the procedure to fit Eq. (3) to the data in Appendix B. Here, we focus on the analysis of the plateau value A

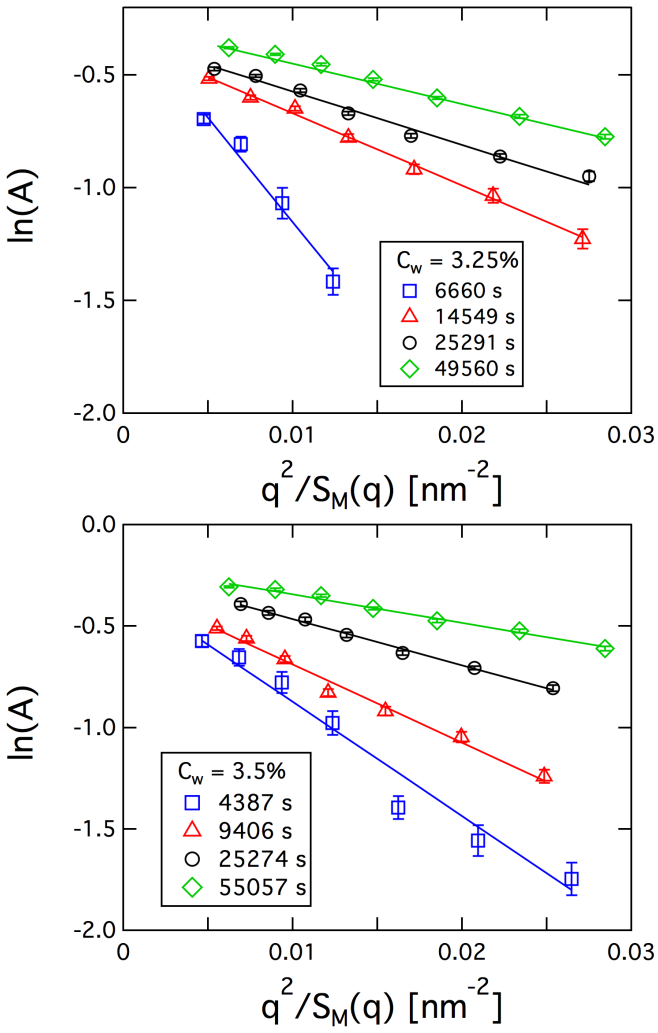

FIG. 3. Logarithm of the intermediate plateau value A of the dynamic structure as a function of the wave-vector squared divided by the measurable structure factor of suspensions with (a) $C_w = 3.25$ wt% and (b) $C_w = 3.5$ wt% at various ages indicated in the legends. The lines depict the results of fits using a Debye-Waller relation (Eq. (4)).

and its implications for the ergodic to non-ergodic transition in the suspensions.

As mentioned above, the emergence of a plateau in the correlation function at the end of the fast relaxation results from the fact that the particles become localized within the cages formed by their neighbors. The plateau value at different wave vectors is well described by a Debye-Waller relation that includes a correction due to de Gennes narrowing [44],

$$A = f_0 \exp\left(-q^2 r_{loc}^2 / 6 S_M(q)\right) \tag{4}$$

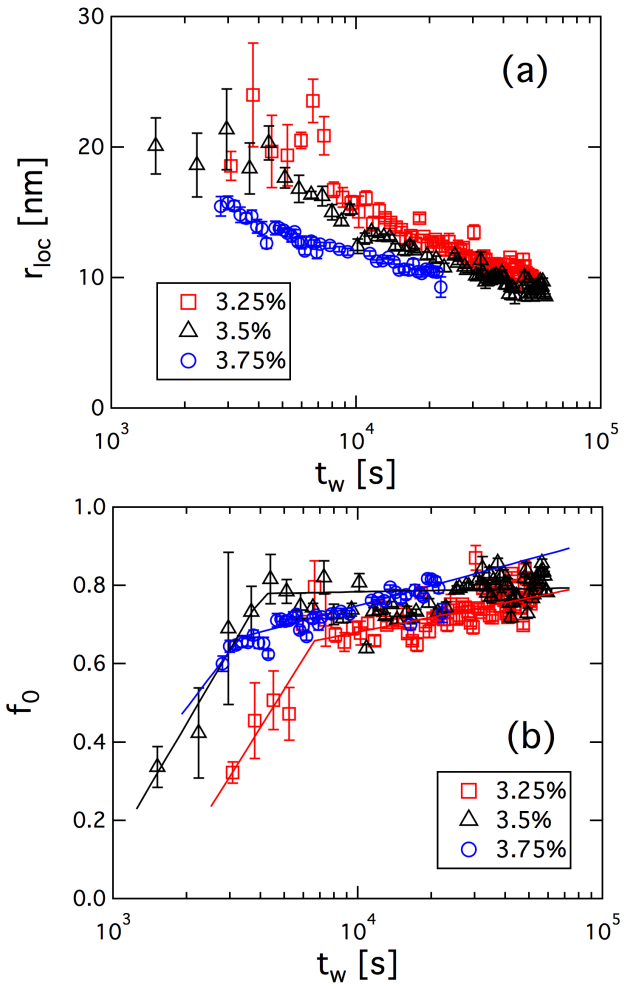

FIG. 4. (a) Localization length r_{loc} and (b) localized fraction f_0 as a function of age for suspensions with concentrations $C_w = 3.25$ wt% (squares), 3.5 wt% (triangles), and 3.75 wt% (circles). The solid lines in (b) show the results of fits using piece-wise logarithmic functions.

where r_{loc} is the average localization length, the prefactor f_0 is the non-ergodicity parameter in the limit $q \to 0$, which is equivalent to the fraction of particles that are localized [45], and $S_M(q)$ is the measurable structure factor, which is the approximation to the structure factor that we can determine experimentally, as described in Appendix A. Figures 3(a) and (b) show $\ln(A)$ versus q^2 at different ages of the suspensions with $C_w = 3.25$ wt% and 3.5 wt%, respectively, where the solid lines depict the results of fits using Eq. (4). The parameters r_{loc} and f_0 obtained from the fits show strong age dependence, as depicted in Fig. 4. Consistent with previous studies [20, 30, 31], the localization length r_{loc} decreases steadily with age indicating increasingly restricted localized motion of the particles with increasing age. One

interpretation for this decrease identified previously is a growth in the interparticle repulsion with increasing age [30]. At late ages, the rate of decrease becomes slow, and the average range of this localized motion reaches approximately 10 nm, which is approximately one-fifth the nearest-neighbor spacing of the disk-shaped Laponite particles (see Appendix A).

The growth of f_0, as shown in Fig. 4(b), indicates that the fraction of localized particles increases with age. This growth is approximated by a piece-wise logarithmic function, depicted by the lines in Fig. 4(b), that divides the age dependence into two stages. In the first stage, the population of localized particles grows rapidly from a small fraction to about 60% to 70% of the total, while in the second stage, when most of the particles are localized, the fraction increases more slowly. The fact that f_0 remains less than one at all ages implies a persistent fraction of "free" particles moving rapidly over a large distance [46, 47]. Colloidal concentration has a clear effect on the rate of the localization process, where more particles become arrested at a faster pace in suspensions with a higher colloidal concentration. Note that the data in Fig. 3(b) for the suspension with $C_w = 3.5$ wt% at age $t_w = 25274$ s falls in the interval of the rejuvenation tests but shows no difference in behavior from the other data. Although the evolution of the shear modulus of the suspension with $C_w = 3.5$ wt% was interrupted by the rejuvenation tests, as seen in Fig. 1, the nature of the localization was apparently unaffected by the macroscopic deformation.

This particle localization constitutes a microscopic signature of the loss of ergodicity that underlies the fluid-solid transition observed macroscopically by the development of an elastic shear modulus like in Fig. 1. Theoretical efforts have sought to make concrete connections between the attainment of macroscopic elasticity and microscopic localization in disordered solids [11, 33, 48–53]. For instance, naive mode coupling theory (NMCT), which describes the dynamics of a single particle driven by the mean force exerted by the surrounding liquid and its localization through a Langevin equation of motion, predicts that for a system of spherical colloids with effectively hard-core interactions, the shear modulus and the localization length follow the scaling relation

$$\frac{G'}{k_B T \rho} = \frac{3\sigma^2}{10 r_{loc}^2}. \tag{5}$$

where ρ is the number density of colloids, σ is the diameter of the spherical colloids, and $k_B T$ is the thermal energy [33, 34]. This prediction of NMCT has previously been shown to relate successfully r_{loc} and G' for two types of concentrated suspensions of spherical nanocolloids

with short-range attractions that form gels with age-dependent properties: one composed of octydecyl-functionalized silica colloids that gel thermo-reversibly in decalin [35] and the other aqueous suspensions of casein micelles that gel through a polymer-induced depletion interaction [36].

To test the possible applicability of the NMCT prediction for relating r_{loc} and G' of the suspensions of disk-shaped Laponite particles, we construct a modified form of the scaling relation in Eq. (5). First, for the number density we take $\rho = \phi/v_0$, where ϕ is the volume fraction and $v_0 = \pi R_L^2 h$ is the volume of a single Laponite particle with thickness $h = 1$ nm and radius $R_L = 15$ nm. Second, we note that the diameter σ enters Eq. (5) to normalize r_{loc} as an approximation for interparticle spacing of the hard spheres considered in the NMCT. To provide an equivalent normalization for the Laponite, we approximate the interparticle spacing by $2\pi/q_p$ where q_p is the position of the first peak in the measurable structure factor of the Laponite suspensions, which varies between 0.123 nm^{-1} and 0.126 nm^{-1} among the three concentrations, corresponding to a nearest neighbor separation of approximately 50 nm (see Appendix A for details). With these modifications, the NMCT scaling prediction becomes

$$\frac{G' v_0}{k_B T} = \frac{6\pi^2 \phi}{5 r_{loc}^2 q_p^2}. \tag{6}$$

We test this prediction by plotting in Fig. 5(a) the left-hand side of Eq. (6), where G' is obtained from the rheometry measurements, together with the right-hand side, where r_{loc} is obtained from the XPCS measurements. As the figure demonstrates, the two quantities track each other closely at later age. At early age the two diverge from one another, with r_{loc}^2 being smaller than expected given the small values of G'. This discrepancy at early ages and the near quantitative agreement at late ages are further illustrated in Fig. 5(b), which displays the ratio of the left-hand and right-hand sides of Eq. (6) as a function of age. The arrows in Fig. 5 indicate the ages at each concentration at which the growth of f_0 changes from rapid growth to slower growth (*i.e.*, the arrows indicate the ages at which the straight lines in Fig. 4(b) intersect). At $C_w = 3.25$ wt% and 3.5 wt%, the period in which Eq. (6) holds appears approximately to coincide with the later stage in the growth of f_0 that we identify with aging of the soft glass, when the fraction of localized particles is large and slowly increasing, and the period in which the scaling breaks down appears approximately to coincide with the earlier stage that we identify with formation. At $C_w =$

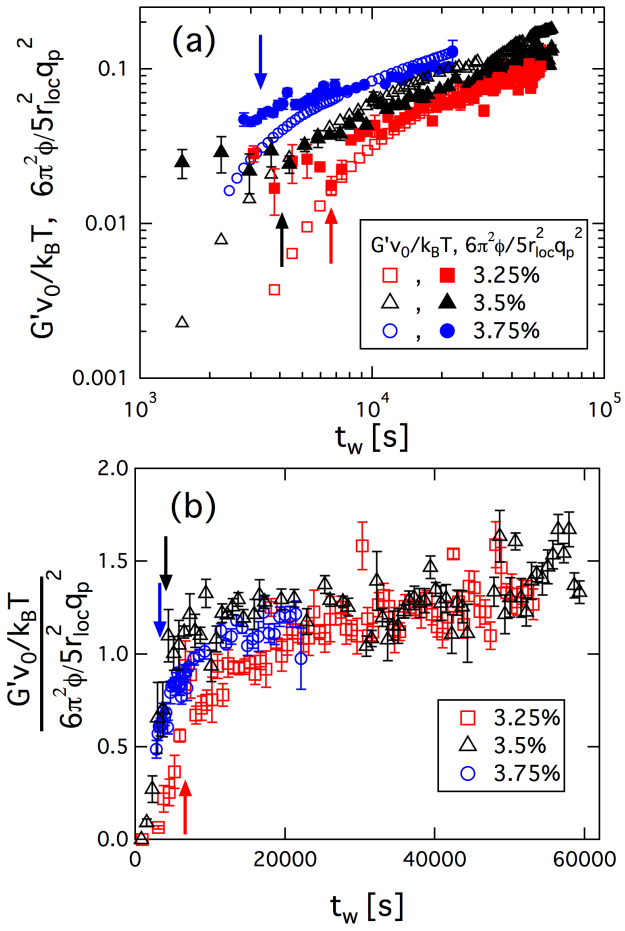

FIG. 5. (a) $G'v_0/k_BT$ (open symbols) and $6\pi^2\phi/5r_{loc}^2q_p^2$ (closed symbols), the two sides of Eq. (6), as functions of age, and (b) the ratio of the two sides of Eq. (6) as a function of age for suspensions with concentrations $C_w = 3.25$ wt% (squares), 3.5 wt% (triangles), and 3.75 wt% (circles). The arrows indicate the ages of the crossing points between faster and slower logarithmic growth of f_0 depicted by the solid lines in Fig. 4(b).

3.75 wt%, where the formation and aging proceed fastest, agreement with Eq. (6) is seen only after the crossover.

The collapse of the rheology and XPCS data sets in Fig. 5 at later ages for all three concentrations indicates that the evolution of rigidity of the Laponite soft solids originates in the localization of the particles, which experience increasingly restricted caged motion during aging. The success of the NMCT prediction in capturing this connection is remarkable in light of the assumptions and approximations that enter the derivation of Eq. (5), which focuses on dense suspensions in a "ultralocal limit" of hard-core collisions [34]. The unexpected

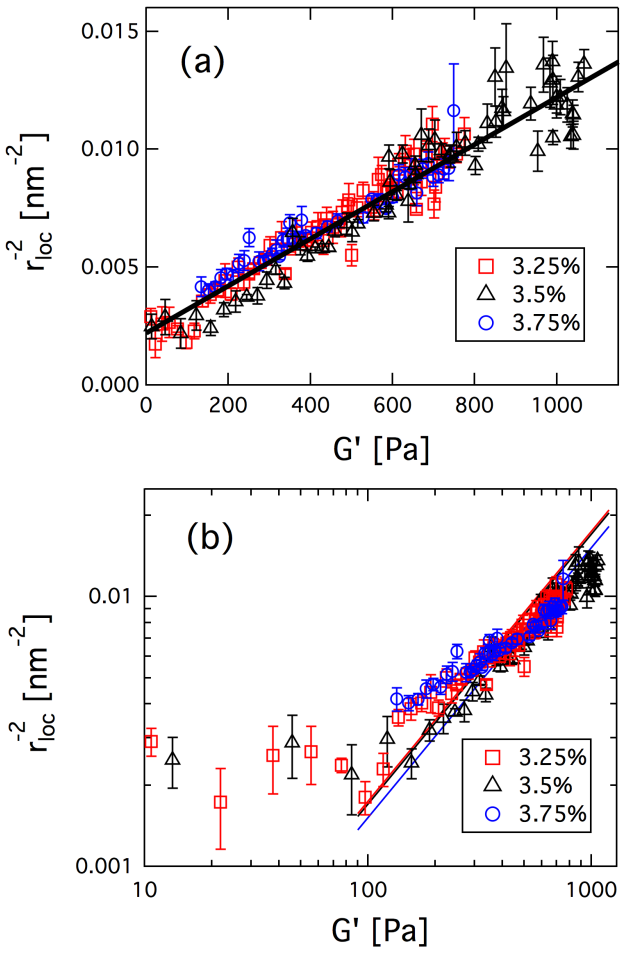

FIG. 6. Inverse of the localization length squared, $1/r_{loc}^2$, versus the storage modulus of the three suspensions plotted on (a) linear and (b) logarithmic scales. The line in (a), which depicts the result of a linear fit to all points, has an intercept of 0.002 nm^{-2} and a slope of 1.0×10^{-5} nm^{-2}Pa^{-1}. The red, black, and blue lines in (b) show the relation between r_{loc}^{-2} and G' obtained from NMCT (Eq. (6)) for the suspensions with $C_w = 3.25$ wt%, 3.5 wt%, and 3.75wt%, respectively.

success of Eq. (6) in connecting the microscopic dynamics and elasticity of the Laponite suspensions, which are composed of a relatively small volume fraction of disk-shaped particles interacting through screened Coulomb forces, suggests this theoretical approach has broader validity than previously appreciated. The breakdown of Eq. (6) at early ages can be understood if one infers from the small and rapidly changing values of f_0 at these ages that the dynamics during this initial period are strongly influenced by heterogeneity, which a mean-field theory like NMCT cannot be expected to capture.

Another perspective from which to evaluate the connection between the evolving elasticity of the Laponite suspensions and the particle localization is to consider the strong variation in the rate of soft-solid formation and aging at different concentrations. As shown in Figs. 1 and 4(a), the timescales over which G' increases and r_{loc} decreases become shorter as the concentration increases. As shown in Fig. 6(a), despite this variation, when plotted against each other, G' and r_{loc}^{-2} for all three concentrations collapse onto a single curve. That is, a one-to-one correspondence exists between G' and r_{loc}, independent of concentration, over the full range of sample ages. For reference, the NMCT prediction for the relation between G' and r_{loc}^{-2} given by Eq. (6) is shown by the lines in the log-log representation of the data in Fig. 6(b). The measured results approach the NMCT predictions as the localization length becomes significantly smaller than the diameter of the particles. Further, as demonstrated in Fig. 6(a), G' and r_{loc}^{-2} follow a linear relationship through all ages that appears to asymptote at zero shear modulus to a finite localization length.

A finite localization length at zero shear modulus suggested by Fig. 6(a) indicates dynamic heterogeneity in the suspensions with the formation of clusters of dynamically correlated particles in the colloidal fluid that precedes the creation of any percolating stress-bearing particle configurations. Cluster formation has been observed in many colloidal systems [54, 55], and the formation of clusters in fluid Laponite suspensions has been proposed in interpretations of light scattering results on low-concentration dispersions [56, 57]. Such clusters could form due to attraction between the discoidal particles resulting from their inhomogeneous surface charge or from the failure of some particles to dissociate during preparation of the suspensions [58]. This picture is supported by the observation that only a small fraction of particles is constrained to a finite localization length at early age.

We note, however, while the extrapolation of the data to $G' = 0$ in Fig. 6(a) suggests r_{loc} remains finite, the measurements at the earliest ages were not able to detect a finite r_{loc} before the suspensions first had measurable elasticity ($G' \gtrapprox 0.67$ Pa). Specifically, at these earliest ages, the terminal relaxation in $f^2(q,\tau)$ was too fast and the intermediate plateau was too small to distinguish from statistical noise. An example is $f^2(q,\tau)$ at $t_w = 2352$ s shown in Fig. 2. Thus, another possibility besides a finite localization length at $G' = 0$ is that r_{loc} changes discontinuously at the fluid-solid transition. Note from Fig. 4(a) that the upper bound of measurable r_{loc} is about 20 nm, which is about two-fifths the nearest neighbor separation. This length could reflect an upper limit in a Lindemann-type criterion

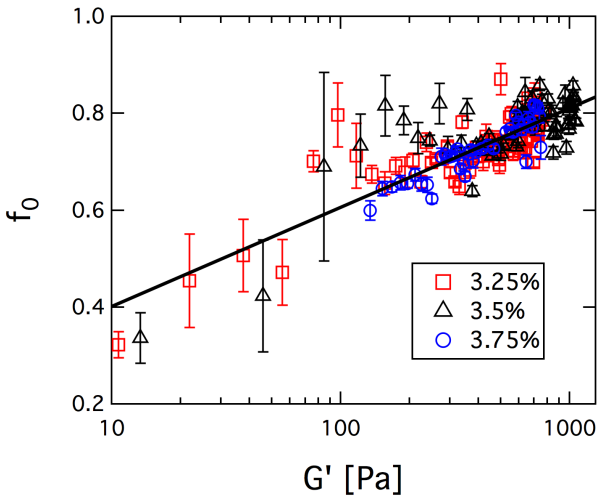

FIG. 7. f_0, the non-ergodicity parameter in the limit $q \to 0$, as a function of shear modulus. The solid line is a logarithmic fit to all points, $f_0 = c \ln G' + b$, with $c = 0.089$ and $b = 0.20$ with G' measured in unit of Pa.

for the glass stability [59]. To resolve better experimentally the dynamics in this regime of large localization length would require XPCS measurements at short delay time with better statistics and at smaller wave vector than we achieved in this experiment.

The intimate connection between particle localization and suspension elasticity can be also seen by comparing the localized fraction f_0 with G', as shown in Fig. 7. Like with r_{loc} versus G' in Fig. 6, values of f_0 for all three suspension concentrations collapse onto a single master curve when plotted against G' despite the strongly differing rates of aging. In particular, one sees from Fig. 7 that f_0 varies approximately logarithmically with G' over the full range of the data. Further, one can extrapolate this dependence to the theoretical limit in which all the particles are arrested ($f_0 = 1$) to predict a maximum shear modulus of the Laponite suspensions in the range 11-12 kPa. More broadly, the surprising scaling between both r_{loc} and G' shown in Fig. 6 and that between f_0 and G' in Fig. 7, independent of the particle concentration, suggests that the mechanical response of Laponite suspensions relies on local properties like the size of the cage rather than the number of particles, so that the increase in concentration only hastens the pace of soft-glass formation and aging, but ultimately does not alter quantitatively the attainment of elasticity.

IV. CONCLUSION

In conclusion, this study employing rheo-XPCS to relate the microscopic and macroscopic manifestations of the fluid-to-solid transition and aging behavior of Laponite suspensions has uncovered a number of unexpected findings that should motivate further research. First, with the success of the NMCT scaling relation in connecting the microscopic localization length and macroscopic shear modulus of the suspensions at late ages demonstrated in Fig. 5, Laponite joins a growing list of non-ergodic colloidal solids for which this theoretical prediction has quantitative validity. As mentioned above, materials previously shown to follow the NMCT prediction were concentrated suspensions of nanospheres that formed gels through short-range attraction [35, 36]. One possible explanation for the similarity in the behavior of Laponite with these systems is that the Laponite dispersions also form gels through similar short-range attractions. This conclusion, while potentially consistent with recent results supporting gel formation by Laponite [60], contradicts the prevailing picture that the non-ergodic state in the range of concentrations studied here is a repulsive glass [17]. In any case, the interparticle interactions of Laponite, with its anisotropic shape and spatially heterogeneous surface charge, are more complex than those of nanospheres with short-range attraction. Hence, an alternative, more intriguing explanation is that the similarity between Laponite and the other materials implies the NMCT prediction has universality, perhaps derived from the mean-field nature of the theory, that makes it insensitive to microscopic details. Studies of other attractive and repulsive non-ergodic colloidal solids that test the range of applicability of the NMCT prediction would help clarify this issue.

Second, the rheo-XPCS experiments have provided a microscopic view of the very earliest stages in the development of the Laponite suspensions that suggests a process by which the particle dynamics evolve on approaching non-ergodicity. The small fraction of localized particles observed at early ages implies strong dynamic heterogeneity in the incipient soft-solid state. As described above, the results suggest this heterogeneous localization precedes the attainment of macroscopic elasticity; however, the measurements are ultimately unable to demonstrate this sequence conclusively. Further experiments that focus on this question would potentially provide significant insight into the nature of the ergodic to non-ergodic transition in Laponite and other nanocolloidal suspensions. A promising direction for such studies would be to examine Laponite suspensions with concentrations that are lower than

those studied here but still in the range where repulsive interactions dominate, since the rates of formation and aging can be expected to be slower, facilitating close study of the early-age behavior. Measurements on such low-concentration suspensions that combine XPCS and with *in situ* rheometry like those reported here, and that hence relate the microscopic and macroscopic properties unambiguously, would be particularly fruitful.

V. ACKNOWLEDGEMENTS

Funding was provided by the NSF (CBET-1804721) and the NSERC Discovery grant program. The research used resources of the Advanced Photon Source and the Center for Nanoscale Materials, U.S. Department of Energy (DOE) Office of Science User Facilities operated for the DOE Office of Science by Argonne National Laboratory under Contract No. DE-AC02-06CH11357.

VI. APPENDIX A: MEASURABLE STRUCTURE FACTOR OF LAPONITE SUSPENSIONS

Figure 8(a) shows the scattering intensity $I(q)$ of the three Laponite suspensions obtained at late age with the Rigaku detector, averaged over wave-vector directions and summed over 100000 frames. For reference, the background scattering intensity measured on the empty Couette cell is also shown. The inset to Fig. 8(b) shows the form factor $\langle F(q)\rangle$ calculated for a disk with 30 nm diameter and 1 nm thickness, averaged uniformly over orientations. Figure 8(b) displays the "measurable" structure factor, $S_M(q) = CI(q)/\langle F(q)\rangle$ where C is a normalization constant, of the suspension with 3.25 wt% at different ages. We determine C by requiring that $S_M(q)$ converges to one at large q. We emphasize that $S_M(q)$ is only an approximation to the true structure factor due to the orientational correlations that likely exist between neighboring particles and to potential polydispersity of the Laponite particles [61]. The peak in the measurable structure factor, which corresponds to nearest neighbor positional correlations, gradually decreases in height with increasing age, but its position, indicated by the arrow in Fig. 8(b), remains roughly unchanged at $q \approx 0.123$ nm^{-1}. At concentrations 3.5 wt% and 3.75 wt%, the peak position was 0.126 and 0.123 nm^{-1}, respectively, again independent of age. Note the measurable structure factor is truncated at $q = 0.2$ nm^{-1} because its shape at higher q is strongly influenced by details in $\langle F(q)\rangle$ and thus not trustworthy.

VII. APPENDIX B: PROCEDURE FOR FITTING $f^2(q,t)$ AND RESULTS FOR THE TERMINAL RELAXATION

Figure 9(a) shows the stretching exponents β, obtained from fits using Eq. (3), describing the shape of the terminal relaxation at $q = 0.07$ nm^{-1} as functions of age for the three concentrations. The exponent at concentrations $C_w = 3.25$ wt% and 3.5 wt% shows an initial growth until around $t_w = 16000$ s and 15000 s, respectively. In the XPCS measurements on the $C_w = 3.75$ wt% sample, the LAMBDA detector was employed only at ages greater than $t_w = 7111$ s. Consequently, the terminal relaxation was not characterized at earlier ages at this concentration, and this initial behavior was not captured. The stretching exponents of all ages remain less than one, which is consistent with previous studies of spontaneous

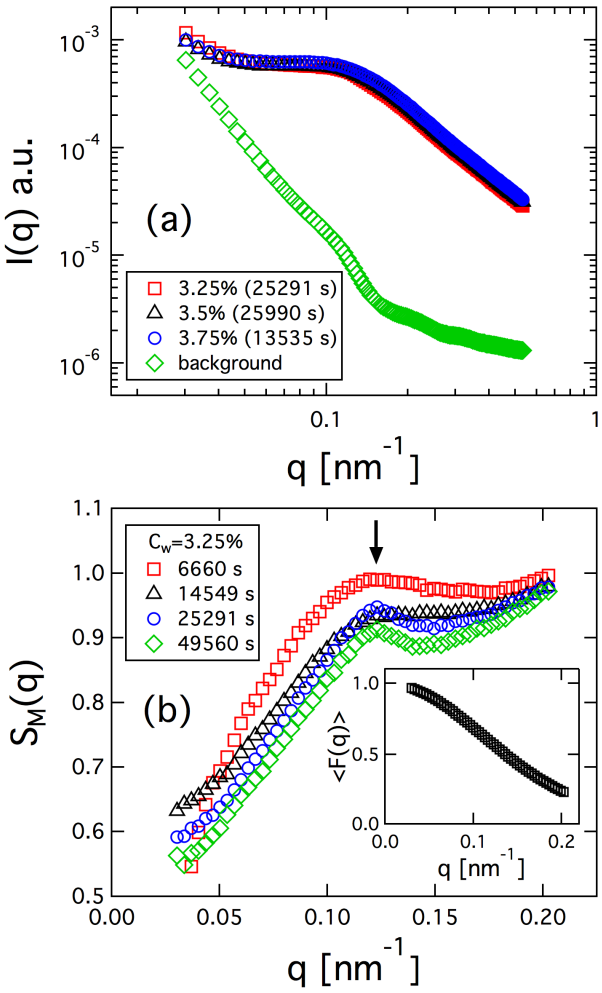

FIG. 8. (a) Scattering intensity $I(q)$ of the Laponite suspensions at the three concentrations at late age and of the empty Couette cell obtained with the Rigaku detector. The intensity is averaged over wave-vector direction and summed over 100000 frames. (b) Measurable structure factor $S_M(q)$ of the suspension with $C_w = 3.25$ wt% at different ages. The arrow at $q = 0.123$ nm^{-1} indicates the position of the interparticle structure factor peak. The inset shows the theoretical form factor $\langle F(q)\rangle$ of a disk with 30 nm diameter and 1 nm thickness, averaged uniformly over orientations.

aging of Laponite suspensions [62, 63]. At later ages, the exponent shows no discernible age dependence. Therefore, at later ages, we performed the fits to $f^2(q,t)$ using Eq. (3) in two steps. First, we allowed β to float, then in a second round of fitting we fixed it at its average for $t_w > 15982$, 15140, and 7111 s for the suspensions with $C_w = 3.25$ wt%, 3.5 wt%, and 3.75 wt%, respectively, to reduce the scatter in the other fit parameters.

As shown in Fig. 9(b), the relaxation time τ_2 of the terminal relaxation experiences

exponential growth, $\tau_2 \propto \exp(at_w)$, at early age and then increases approximately linearly with age, $\tau_2 \propto t_w^{\delta}$ with $\delta \approx 1$, at later age. The transient decrease of τ_2 and increase of β near $t_w = 35000$ s at concentration $C_w = 3.5$ wt% are consequences of the rejuvenation induced by the steady shear applied immediately prior to that time. A similar sequence of exponential followed by linear growth of τ_2 has been observed previously [27, 29]. This change in age dependence has been identified as a transition in the microscopic dynamics associated with the slow relaxation from colloidal diffusion to cage hopping [32], and the two periods have been referred to "cage-forming" and "full-aging" regimes, respectively [27–29]. The evolution in the slow relaxation with age is further seen in the wave-vector dependence of τ_2, which is shown in Fig. 10(a) and (b) for $C_w = 3.25$ wt% and $C_w = 3.5$ wt%, respectively, at various ages. The relaxation time varies approximately as a power law with wave vector, $\tau_2 \sim q^{-\alpha}$. At early age, $\alpha \approx 2$, which is interpreted in terms of slow diffusion associated with cage breaking, while at later ages $\alpha \approx 1$, which has been modeled in terms of activated hopping [32, 64] or slow strain motion in response to heterogeneous stress relaxation in the glassy matrix [30].

The relaxation time τ_1 characterizing the fast dynamics associated with the first partial decay of $f^2(q,\tau)$ remains less than of order 10^{-4} s at all ages for all three concentrations. However, as seen in Fig. 2, the experimental range of delay time τ captures only the tail end of the first decay, and $f^2(q,\tau)$ has considerable scatter at short τ; hence, the values of τ_1 have a large uncertainty.

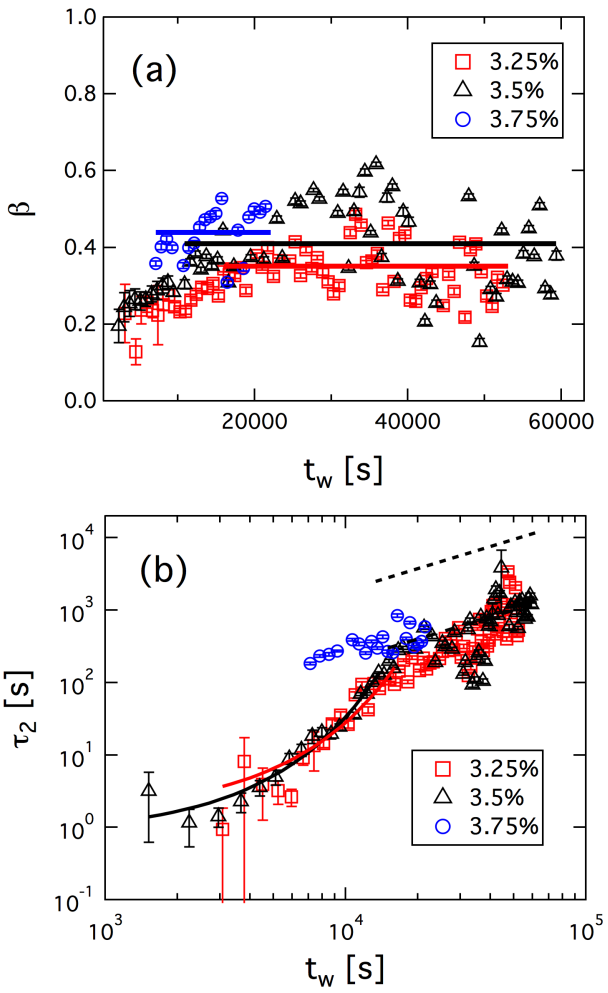

FIG. 9. (a) Stretching exponent β characterizing the shape of the terminal relaxation in $f(q,\tau)$ at $q = 0.07$ nm^{-1} as a function of age obtained from fits using Eq. (3) for the three Laponite concentrations. The solid horizontal lines show the mean values $\bar{\beta}$ at late ages used in fits to obtain other parameters in Eq. (3). Specifically, $\bar{\beta}(C_w = 3.25$ wt%$) = 0.35$, $\bar{\beta}(C_w = 3.5$ wt%$) = 0.41$, and $\bar{\beta}(C_w = 3.75$ wt%$) = 0.44$. (b) Relaxation time τ_2 characterizing the terminal decay in $f(q,\tau)$ at $q = 0.077$ nm^{-1} as a function of age. The solid lines are exponential fits to τ_2 at early age, $\tau_2 = \tau_0 e^{at_w}$, where $\tau_0 = 1.5$ s and $a = 2.9 \times 10^{-4}$ s^{-1} for $C_w = 3.25$ wt%, and $\tau_0 = 0.79$ s and $a = 3.7 \times 10^{-4}$ s^{-1} for $C_w = 3.5$ wt%. The dashed line has slope of 1.

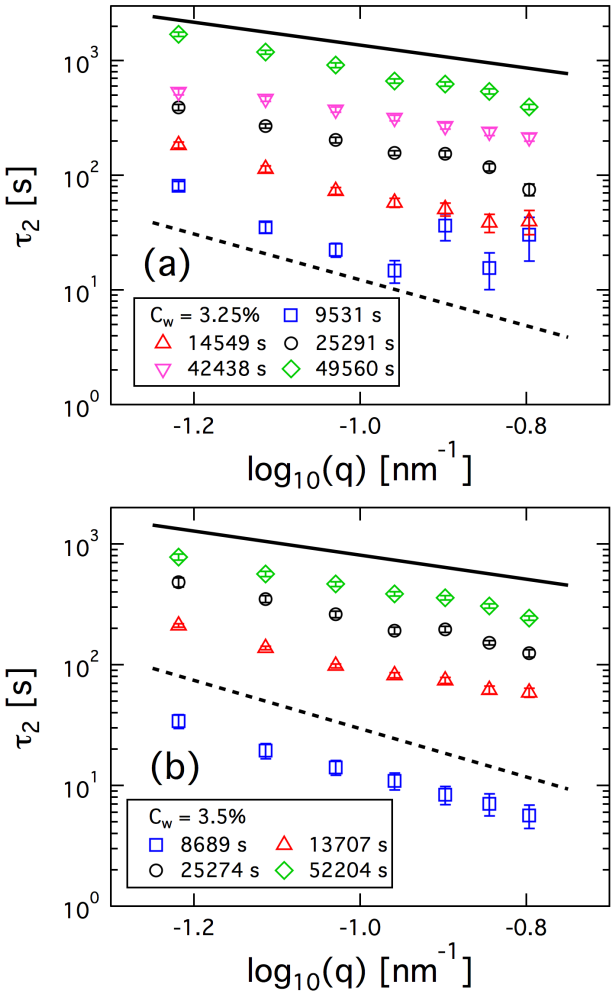

FIG. 10. The terminal relaxation time τ_2 of the dynamic structure factor as a function of wave vector of suspensions with (a) $C_w = 3.25$ wt% and (b) $C_w = 3.5$ wt% at various ages indicated in the legends. The solid lines in both panels have slope of -1, and the dashed lines have slope of -2.

[1] G. L. Hunter and E. R. Weeks, Reports on Progress in Physics **75**, 066501 (2012).

[2] E. Zaccarelli, Journal of Physics: Condensed Matter **19**, 323101 (2007).

[3] E. Zaccarelli, in Proceedings of the International School of Physics "Enrico Fermi", Vol. 84, Physics of Complex Colloids, edited by C. Bechinger, F. Sciortino, and P. Ziherl (IOS Press, Amsterdam, 2013) pp. 95 – 154.

[4] C. P. Royall and S. R. Williams, Physics Reports **560**, 1 (2015).

[5] V. A. Martinez, G. Bryant, and W. van Megen, Phys. Rev. Lett. **101**, 135702 (2008).

[6] Y. M. Joshi and G. Petekidis, Rheol. Acta **57**, 521 (2018).

[7] A. R. Jacob, E. Moghimi, and G. Petekidis, Physics of Fluids **31**, 087103 (2019).

[8] A.-M. Philippe, D. Truzzolillo, J. Galvan-Myoshi, P. Dieudonné-George, V. Trappe, L. Berthier, and L. Cipelletti, Phys. Rev. E **97**, 040601(R) (2018).

[9] V. Trappe and P. Sandkuhler, Current Opinion in Colloid & Interface Science **8**, 494 (2004).

[10] P. J. Lu, E. Zaccarelli, F. Ciulla, A. B. Schofield, F. Sciortino, and D. A. Weitz, Nature **453**, 499 (2008).

[11] A. H. Krall and D. A. Weitz, Phys. Rev. Lett. **80**, 778 (1998).

[12] T. G. Mason and D. A. Weitz, Phys. Rev. Lett. **75**, 2770 (1995).

[13] C. J. Rueb and C. F. Zukoski, Journal of Rheology **42**, 1451 (1998).

[14] A. Mourchid, A. Delville, J. Lambard, E. LeColier, and P. Levitz, Langmuir **11**, 1942 (1995).

[15] S. Bhatia, J. Barker, and A. Mourchid, Langmuir **19**, 532 (2003).

[16] P. Levitz, E. Lecolier, A. Mourchid, A. Delville, and S. Lyonnard, Europhysics Letters (EPL) **49**, 672 (2000).

[17] B. Ruzicka and E. Zaccarelli, Soft Matter **7**, 1268 (2011).

[18] B. Ruzicka, L. Zulian, and G. Ruocco, Langmuir **22**, 1106 (2006).

[19] R. Angelini, E. Zaccarelli, F. A. de Melo Marques, M. Sztucki, A. Fluerasu, G. Ruocco, and B. Ruzicka, Nature Communications **5**, 4049 (2014).

[20] D. Bonn, H. Tanaka, G. Wegdam, H. Kellay, and J. Meunier, Europhysics Letters (EPL) **45**, 52 (1999).

[21] S. Jabbari-Farouji, E. Eiser, G. H. Wegdam, and D. Bonn, Journal of Physics: Condensed Matter **16**, L471 (2004).

[22] H. A. Baghdadi, J. Parrella, and S. R. Bhatia, Rheologica Acta **47**, 349 (2008).

[23] D. Saha, Y. M. Joshi, and R. Bandyopadhyay, Soft Matter **10**, 3292 (2014).

[24] A. Shahin and Y. M. Joshi, Langmuir **28**, 15674 (2012).

[25] N. Willenbacher, Journal of Colloid and Interface Science **182**, 501 (1996).

[26] K. Suman and Y. M. Joshi, Langmuir **34**, 13079 (2018).

[27] M. Bellour, A. Knaebel, J. L. Harden, F. Lequeux, and J.-P. Munch, Phys. Rev. E **67**, 031405 (2003).

[28] H. Tanaka, S. Jabbari-Farouji, J. Meunier, and D. Bonn, Phys. Rev. E **71**, 021402 (2005).

[29] F. Schosseler, S. Kaloun, M. Skouri, and J. P. Munch, Phys. Rev. E **73**, 021401 (2006).

[30] R. Bandyopadhyay, D. Liang, H. Yardimci, D. A. Sessoms, M. A. Borthwick, S. G. J. Mochrie, J. L. Harden, and R. L. Leheny, Phys. Rev. Lett. **93**, 228302 (2004).

[31] R. Angelini, A. Madsen, A. Fluerasu, G. Ruocco, and B. Ruzicka, Colloids and Surfaces A: Physicochemical and Engineering Aspects **460**, 118 (2014).

[32] F. A. D. M. Marques, R. Angelini, E. Zaccarelli, B. Farago, B. Ruta, G. Ruocco, and B. Ruzicka, Soft Matter **11**, 466 (2015).

[33] Y.-L. Chen and K. S. Schweizer, The Journal of Chemical Physics **120**, 7212 (2004).

[34] K. S. Schweizer and G. Yatsenko, The Journal of Chemical Physics **127**, 164505 (2007).

[35] H. Guo, S. Ramakrishnan, J. L. Harden, and R. L. Leheny, Phys. Rev. E **81**, 050401(R) (2010).

[36] N. Mahmoudi and A. Stradner, Soft Matter **13**, 4629 (2017).

[37] Y. Chen, S. A. Rogers, S. Narayanan, J. L. Harden, and R. L. Leheny, Phys. Rev. Materials **4**, 035602 (2020).

[38] D. Pennicard, S. Lange, S. Smoljanin, J. Becker, H. Hirsemann, M. Epple, and H. Graafsma, Journal of Instrumentation **6**, C11009 (2011).

[39] F. Khan, S. Narayanan, R. Sersted, N. Schwarz, and A. Sandy, Journal of Synchrotron Radiation **25**, 1135 (2018).

[40] J. D. Ferrara, Y. Nakaye, Y. Sakuma, S. Mikusu, and T. Sakumura, Acta Crystallographica Section A **75**, a74 (2019).

[41] R. L. Leheny, M. C. Rogers, K. Chen, S. Narayanan, and J. L. Harden, Current Opinion in Colloid & Interface Science **20**, 261 (2015).

[42] M. Mours and H. H. Winter, Rheologica Acta **33**, 385 (1994).

[43] W. van Megen and S. M. Underwood, Phys. Rev. Lett. **70**, 2766 (1993).

[44] J. P. Hansen and I. R. McDonald, Theory of simple liquids (Academic Press, 1976).

[45] H. Guo, S. Ramakrishnan, J. L. Harden, and R. L. Leheny, The Journal of Chemical Physics **135**, 154903 (2011).

[46] S. Jabbari-Farouji, H. Tanaka, G. H. Wegdam, and D. Bonn, Phys. Rev. E **78**, 061405 (2008).

[47] S. Jabbari-Farouji, G. H. Wegdam, and D. Bonn, Phys. Rev. Lett. **99**, 065701 (2007).

[48] C. L. Klix, F. Ebert, F. Weysser, M. Fuchs, G. Maret, and P. Keim, Phys. Rev. Lett. **109**, 178301 (2012).

[49] J. Bergenholtz, W. C. K. Poon, and M. Fuchs, Langmuir **19**, 4493 (2003).

[50] A. Zaccone and E. M. Terentjev, Phys. Rev. Lett. **110**, 178002 (2013).

[51] H. Yoshino and F. Zamponi, Phys. Rev. E **90**, 022302 (2014).

[52] A. Ikeda and L. Berthier, Phys. Rev. E **92**, 012309 (2015).

[53] E. Flenner and G. Szamel, Phys. Rev. Lett. **114**, 025501 (2015).

[54] P. N. Segrè, V. Prasad, A. B. Schofield, and D. A. Weitz, Phys. Rev. Lett. **86**, 6042 (2001).

[55] P. J. Lu, J. C. Conrad, H. M. Wyss, A. B. Schofield, and D. A. Weitz, Phys. Rev. Lett. **96**, 028306 (2006).

[56] F. Pignon, J.-M. Piau, and A. Magnin, Phys. Rev. Lett. **76**, 4857 (1996).

[57] T. Nicolai and S. Cocard, Langmuir **16**, 8189 (2000).

[58] H. Z. Cummins, Journal of Non-Crystalline Solids **353**, 3891 (2007).

[59] X. Yang, H. Tong, W.-H. Wang, and K. Chen, Phys. Rev. E **99**, 062610 (2019).

[60] K. Suman and Y. M. Joshi, Langmuir **34**, 13079 (2018).

[61] F. Scheffold and T. G. Mason, Journal of Physics: Condensed Matter **21**, 332102 (2009).

[62] B. Abou, D. Bonn, and J. Meunier, Phys. Rev. E **64**, 021510 (2001).

[63] R. Angelini, L. Zulian, A. Fluerasu, A. Madsen, G. Ruocco, and B. Ruzicka, Soft Matter **9**, 10955 (2013).

[64] R. Angelini and B. Ruzicka, Colloids and Surfaces A: Physicochemical and Engineering Aspects **483**, 316 (2015).